THE JOURNAL OF BIOLOGICAL CHEMISTRY VOL. 287, NO. 6, pp. 4157–4164, February 3, 2012

Kinetics of the Association/Dissociation Cycle of an ATP-binding Cassette Nucleotide-binding Domain*[S]

Received for publication, October 28, 2011, and in revised form, December 7, 2011 Published, JBC Papers in Press, December 9, 2011, DOI 10.1074/jbc.M111.318378

Maria E. Zoghbi, Kerry L. Fuson, Roger B. Sutton, and Guillermo A. Altenberg[1]

From the Department of Cell Physiology and Molecular Biophysics and Center for Membrane Protein Research, Texas Tech Health Sciences Center, Lubbock, Texas 79430-6551

Background: ATP induces dimerization of the nucleotide-binding domains (NBD) of ATP-binding cassette proteins, followed by ATP hydrolysis and dimer dissociation.
Results: The rate of dimerization induced by MgATP is faster than previously thought.
Conclusion: During the hydrolysis cycle, there is a dynamic equilibrium where neither monomers nor dimers are favored.
Significance: Knowledge of the mechanism of hydrolysis by NBDs will help us understand the function of ATP-binding cassette proteins.

Most ATP binding cassette (ABC) proteins are pumps that transport substrates across biological membranes using the energy of ATP hydrolysis. Functional ABC proteins have two nucleotide-binding domains (NBDs) that bind and hydrolyze ATP, but the molecular mechanism of nucleotide hydrolysis is unresolved. This is due in part to the limited kinetic information on NBD association and dissociation. Here, we show dimerization of a catalytically active NBD and follow in real time the association and dissociation of NBDs from the changes in fluorescence emission of a tryptophan strategically located at the center of the dimer interface. Spectroscopic and structural studies demonstrated that the tryptophan can be used as dimerization probe, and we showed that under hydrolysis conditions (millimolar MgATP), not only the dimer dissociation rate increases, but also the dimerization rate. Neither dimer formation or dissociation are clearly favored, and the end result is a dynamic equilibrium where the concentrations of monomer and dimer are very similar. We proposed that based on their variable rates of hydrolysis, the rate-limiting step of the hydrolysis cycle may differ among full-length ABC proteins.

ABC[2] proteins are ubiquitous membrane proteins that mediate the transport of a wide variety of substrates across membranes. ABC proteins span from bacteria to man (1), and elucidation of their function at the molecular level is essential to understand processes such as multidrug resistance of cancer cells mediated by P-glycoprotein (MDR1, ABCB1) and diseases, such as cystic fibrosis, caused by mutations of the cystic fibrosis transmembrane conductance regulator (CFTR, ABCC7) (1, 2).

The core structure of ABC proteins consists of two transmembrane domains and two NBDs (1). The dissimilar functions of the ABC proteins (ion channel, transporter of lipids, peptides, organic chemicals, etc.) depend on the poorly conserved transmembrane domains, whereas the more conserved NBDs are responsible for the nucleotide binding and hydrolysis (1). In many ABC proteins from lower organisms, the two NBDs are identical (3). In other proteins they have very similar sequences and functional properties (*e.g.* P-glycoprotein) (2, 4), whereas in a minority, one of the NBDs is catalytically defective, and the functional roles of the two NBDs differ (*e.g.* CFTR) (5).

There is general agreement that the two NBDs work as a dimer, but discrepancies in crystal structures, biochemical and biophysical data, and molecular dynamic simulations have led to a number of models to explain the mechanism of nucleotide hydrolysis (6–20). These models can be broadly divided into two groups: 1) Monomer/dimer model. ATP binding induces formation of a dimer with two ATPs sandwiched at the dimer interface. The two composite ATP-binding sites are formed by residues from both NBDs. In this model, ATP hydrolysis is followed by dissociation of the dimers, and the energy that drives the conformational changes for substrate transport (power stroke) is provided by the dimer association/dissociation (7, 9, 10, 12, 16, 18, 21). 2) Constant contact model. The NBDs remain in contact during the hydrolysis cycle, and the power stroke results from smaller conformational changes at the NBD-dimer interface (8, 13–15, 17).

The scarcity of detailed information on the NBDs association and dissociation, including kinetic studies, certainly contributes to the absence of a widely accepted mechanistic model of the nucleotide binding/hydrolysis cycle. In this context, both NBD dimerization and dissociation following ATP hydrolysis have been proposed to be the rate-limiting step of the ABC proteins ATPase cycle (4, 22–24).

Here, we studied the association and dissociation of a prototypical NBD, the *Methanococcus jannaschii* MJ0796 (18, 25).

* This work was supported, in whole or in part, by National Institutes of Health grants R01GM79629 and 3R01GM079629–03S1 and by National Institutes of Health National Center for Research Resources Biomedical Technology Program grant P41RR001209 (to the Stanford Synchrotron Radiation Laboratory Structural Molecular Biology Program). This work was also supported by Cancer Prevention and Research Institute of Texas grant RP101073 (to G. A. A.). The Stanford Synchrotron Radiation Laboratory Structural Molecular Biology Program is supported by the United States Department of Energy Office of Biological and Environmental Research and the National Institute of General Medical Sciences.
[S] This article contains supplemental Figs. 1 and 2 and Tables 1 and 2.
[1] To whom correspondence should be addressed: Department of Cell Physiology and Molecular Biophysics, Texas Tech Health Sciences Center, Lubbock, TX 79430-6551. Tel.: 806-743-2531; E-mail: g.altenberg@ttuhsc.edu.
[2] The abbreviations used are: ABC, ATP-binding cassette; MJ, MJ0796-G174W; MJI, MJ0796-G174W-E171Q (MJI); NBD, nucleotide-binding domain.

MJ0796 is a homolog of *Escherichia coli* LolD, the NBD of the LolCDE transport system that mediates movement of inner-membrane lipoproteins to the outer membrane (26). We developed a robust spectroscopic technique and used it to determine the ATP-dependent NBD monomer/dimer equilibration kinetics. Our results indicate that previous determinations of NBD association rates are underestimates of the true values (measured in catalytically active NBDs in the presence of millimolar MgATP), and that under our experimental conditions, dimer dissociation is slightly favored over dimerization.

EXPERIMENTAL PROCEDURES

Protein Expression and Purification—Two *M. jannaschii* MJ0796 mutants were expressed in *E. coli* and purified: MJ0796-G174W (MJ) and MJ0796-G174W-E171Q (MJI). MJ DNA was synthesized (Genscript, Piscataway, NJ), and the MJI mutant was generated by site-directed mutagenesis. DNAs were cloned into pET19b (EMD Biosciences, Rockland, MA), and sequences were confirmed. Protein expression in *E. coli* BL21-CodonPlus (DE3)-RILP (Agilent Technologies, Santa Clara, CA) was induced with 1 mM isopropyl-β-D-thiogalactopyranoside for 2 h at 37 °C. Proteins were purified by previously described methods (18) with all procedures carried out a 4 °C. Cells were disrupted with a microfluidizer in lysis buffer (50 mM NaCl, 1 mM EDTA, 4 mM DTT, 50 mM Tris/HCl (pH 7.6)) with the addition of 1 mM PMSF. The lysate was centrifuged for 15 min at 30,000 × *g*, and the supernatant was diluted 2-fold with NaCl-free buffer (1 mM EDTA, 1 mM DTT, 50 mM Tris HCl (pH 7.6)) and filtered through a 0.45-μm surfactant-free cellulose acetate syringe filter (Corning, NY) before loading it into a Mono Q anion exchange column (HiPrepQ FF16, GE Healthcare). For elution, [NaCl] was increased linearly from zero to 1 M in a solution with the composition of the lysis buffer except for the [NaCl]. The process yields a highly purified protein that can be used for biochemical and biophysical studies, including crystallization. For some experiments, the preparation purified by anion exchange was subjected to size-exclusion chromatography (Superdex HR200 10/300 GL column, GE Healthcare) to obtain a homogeneous monodisperse pure protein sample (Fig. 1 and supplemental Fig. 1). Fractions containing the recombinant protein were stored at −80 °C. The rate of ATP hydrolysis by MJ determined using [γ-^{32}P]ATP was 0.16 ± 0.01 s, whereas that of MJI under similar conditions was undetectable.

Size Exclusion Chromatography—For size exclusion chromatography analysis, a 50-μl aliquot of purified protein (50 μM), was preincubated with or without ATP for 10 min at room temperature before loading it onto a Superdex 200 10/300 GL gel-filtration column (GE Healthcare). The column preequilibration/elution buffer contained 200 mM NaCl and 50 mM Tris-HCl (pH 7.6) with 1 mM ATP present when indicated. Samples were run at 0.5 ml/min at 4 °C. Proteins of known molecular weight were used for calibration to estimate the monomer and dimer apparent molecular weights.

Tryptophan Fluorescence Measurements—Changes in Trp fluorescence (2 μM protein in 200 mM NaCl, 1 mM EDTA, 10% glycerol, 50 mM Tris/HCl (pH 7.6)) were determined at 20 °C, exciting the sample at 295 nm and recording the fluorescence spectra between 310 and 400 nm (F-7000 spectrofluorometer, Hitachi, Tokyo, Japan).

Stop-flow Experiments—Rapid-mixing experiments were performed on an SX20 stop-flow device (Applied Photophysics, Surrey, UK) with a 20-μl chamber and a dead time < 0.5 ms. Light from a Xe lamp, set to 295 nm with a monochromator, was directed to the sample through a fiber optic, and emitted light that passed through a 340 ± 15 nm band pass filter (Semrock, Rochester, NY) was detected by a photomultiplier in close proximity to the sample chamber. Buffer composition and protein concentration were as described in the previous section.

Crystallization, Diffraction Data Collection, Structure Determination, and Refinement—Crystals were grown at 20 °C by the hanging-drop method using 16% PEG-4000, 10% isopropanol, and 0.1 M Hepes (pH, 8.0), and MJI at 18 mg/ml in 20 mM Na-ATP, 1 mM EDTA, 10% glycerol, 4 mM DTT, and 10 mM Tris (pH 8.0). Data were collected at the Stanford Synchrotron Radiation Laboratory on beamline BL7–1 at a wavelength of 0.98 Å. The data sets were collected at 100 K using an ADSC image plate detector. Data were integrated, reduced, and scaled using HKL-2000. The crystals were indexed in the orthorhombic space group C2 2 21, and the structure was solved by molecular replacement using Phaser on diffraction data collected from one crystal to 1.8 Å (supplemental Table 1). Initial model coordinates were obtained from MJ0796-E171Q (PDB code 1L2T). Model building was done with Coot, and refinement of the model was carried out with PHENIX (phenix.refine: 1.7.1_743) with a random subset of all data set aside for calculation of Rfree (10%). Manual adjustments to the models were carried out with Coot. Once refinement was complete, solvent molecules were assessed followed by manual adjustments. The structure of MJI was verified by examining a simulated annealing omit map generated with PHENIX. There were no residues in disallowed regions of the Ramachandran map. Similar results were obtained from data collections at 2.3 Å resolution using an in-house x-ray source (Rigaku ScreenMachine, The Woodlands, TX). Fig. 3 was rendered with PyMOL.

Data Presentation and Statistics—Data are shown as mean ± S.E., and statistical comparisons were performed by Student's *t* test for unpaired data. $p < 0.05$ in a two-tailed analysis was considered significant. The number of experiments, *n*, corresponds to independent measurements from different preparations.

RESULTS

Dimerization Induced by ATP—In previous publications it has been shown that size exclusion chromatography can be used to detect ATP-dependent dimerization of a catalytically inactive MJ0796 mutant (MJ0796-E171Q) (25). The Glu-171 to Gln mutation greatly reduces ATP hydrolysis and stabilizes the ATP-induced dimer (18, 25). However, wild-type isolated NBDs have not been observed as dimers (25). Here, we studied the catalytically active MJ0796-G174W (MJ) and catalytically inactive MJ0796-E171Q/G174W (MJI). MJ and MJI contain the G174W substitution, introduced in these otherwise Trp-less proteins to detect dimerization spectroscopically (see below). The use of Trp-174 as a potential reporter of NBD dimerization in MJ0796 has been introduced by Moody and Thomas (39).

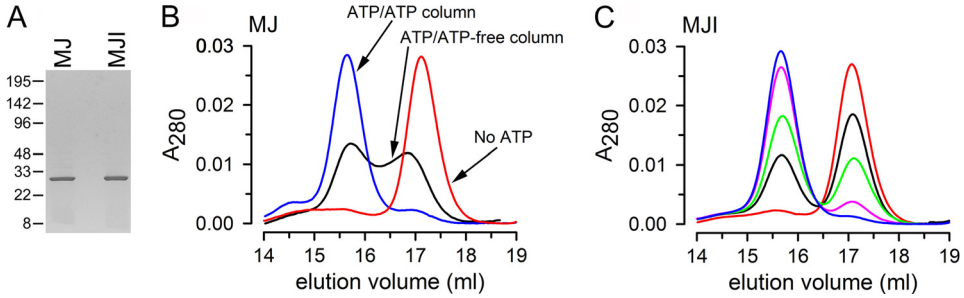

FIGURE 1. **ATP-dependent NBD dimerization.** *A*, Coomassie blue-stained gel of purified MJ and MJI (approximately 3.5 μg of protein per lane). The positions of molecular weight markers are indicated on the left. *B*, gel filtration analysis of purified MJ run as described under "Experimental Procedures." *Red trace* (*No ATP*), MJ equilibrated with 1 mM EDTA and no ATP and eluted without ATP; *blue trace* (*ATP/ATP column*), MJ equilibrated with 1 mM ATP and 1 mM EDTA, injected into the column pre-equilibrated with 1 mM ATP, and eluted with the same solution; *black trace* (*ATP/ATP-free column*), MJ equilibrated with 1 mM EDTA and 1 mM ATP and eluted without ATP. A_{280} is the absorbance measured at 280 nm normalized to the total absorbance area. *C*, gel filtration analysis of purified MJI. MJI was equilibrated with 1 mM EDTA and zero ATP (*red*), 5 μM ATP (*black*), 10 μM ATP (*green*), 20 μM ATP (*pink*), or 40 μM ATP (*blue*). In all cases the column was pre-equilibrated with ATP-free solution without EDTA, a solution also used for elution. See "Experimental Procedures" for details.

We have expressed and purified MJ and MJI (Fig. 1*A*) and evaluated the effect of ATP on their oligomerization state by size exclusion chromatography. In the absence of ATP, MJ eluted as a peak corresponding to the monomeric form of the protein (size estimated at ~28 kDa, *red trace* labeled *No ATP*, Fig. 1*B*). When MJ was preincubated with 1 mM ATP to induce dimerization, and then run on a column in the presence of ATP, it migrated as a single peak corresponding to the dimer (estimated size ~51 kDa, *blue trace* labeled *ATP/ATP column*, Fig. 1*B*). When MJ was preincubated with ATP and then run on an ATP-free column, it eluted as a mix of monomers and dimers (*black trace* labeled *ATP/ATP-free column*, Fig. 1*B*). The appearance of monomers suggests that a proportion of the preformed MJ dimers dissociates during their migration through a column without ATP. In contrast, MJI preincubated with ATP eluted as a dimer even when the column was ATP-free (Fig. 1*C*). Fig. 1*C* also shows that the degree of MJI dimerization depended on the concentration of ATP used during preincubations. The observation that virtually all MJ and MJI monomers become dimers at high ATP concentration indicates that essentially all NBDs in our preparation are competent for ATP binding and dimerization.

We also studied the effect of MgATP during the size exclusion chromatography. MgATP is the preferred MJ hydrolysis substrate. In the presence of MgATP (during preincubation and in the column), MJ migrated as an asymmetric broad peak that significantly overlapped the monomer and dimer peaks (supplemental Fig. 1, *red trace*). We attribute that behavior to rapid, continuous association/dissociation of the NBDs, which alters apparent NBD sizes during the run, resulting in decreased resolution of the monomer and dimer peaks. Direct evidence for a dynamic and rapid MJ monomer/dimer association/dissociation in the presence of saturating MgATP is presented later. Conversely, MJI eluted as a single dimer peak when it was preincubated and run with MgATP (supplemental Fig. 1) or ATP alone (Fig. 1*C*). This Mg-independent migration of ATP-bound MJI dimers is consistent with its very low ATPase activity. In summary, the size exclusion chromatography results show that ATP induces dimerization of both, MJ and MJI, and that, in agreement with previous studies (18, 25), the MJI dimer is more stable than the MJ dimer. The results also show that MJ dimers dissociate following ATP hydrolysis, making MJ a good model for kinetic studies of the monomer/dimer cycle.

Structure of MJI-G174W—We crystallized MJI in the presence of ATP and found it as a dimer (Fig. 2*A*), very similar to the ATP-bound MJ0796-E171Q dimers crystallized previously (18). Data collection and refinement statistics are presented in supplemental Table 1. Crystallization of both proteins was done in the absence of Mg, and the dimers show Na as the cation cofactor. However, instead of ATP, our structure contains two ADPs sandwiched at the dimer interface (*white*, space-filling representation), and P_i (*gray*, space-filling representation). The presence of ADP and P_i indicates that MJI was capable to go through at least one ATP hydrolysis cycle during the crystallization process. In addition, our MJI dimer structure shows clearly the close proximity of the Trp-174 residues (*magenta*, *sticks*) of each monomer at the center of the dimer interface. Fig. 2*B* zooms in on the Trps, showing a π stacking of the Trp rings in a parallel conformation (**1p**) with interatomic distances of 3.0–3.5 Å. This close proximity of the Trps at the dimer interface supports Trp-Trp quenching as the mechanism responsible for the observed decrease in fluorescence during ATP-induced dimerization (see below). Thus, Trp-174 is in an ideal position to monitor NBD dimerization by Trp fluorescence quenching.

Characterization of ATP-induced Changes in Trp174 Fluorescence—In this section, we studied the changes in Trp fluorescence of MJ and MJI in response to ATP under conditions that prevent ATP hydrolysis (nominal absence of Mg and presence of 1 mM EDTA). Addition of a saturating concentration of ATP (2 mM) elicited a Trp fluorescence quenching of about 80% (Fig. 3*A*). Because size-exclusion chromatography shows that all NBDs in our preparation dimerize in response to a high concentration of ATP, we interpret the remaining 20% of the signal as the sum of emission from quenched Trps in dimers, Tyr emission, and/or any small contribution of contaminant proteins. This ATP-insensitive emission was subtracted from the traces presented in the remaining figures. Fig. 3*A* also shows that, in addition to the fluorescence quenching, ATP shifted the emission maximum from ~345 nm (*No ATP*) to ~335 nm (2 mM ATP). Fig. 3*B* shows a representative experiment where Trp fluorescence was quenched by successive increments in ATP concentration, and Fig. 3*C* summarizes the

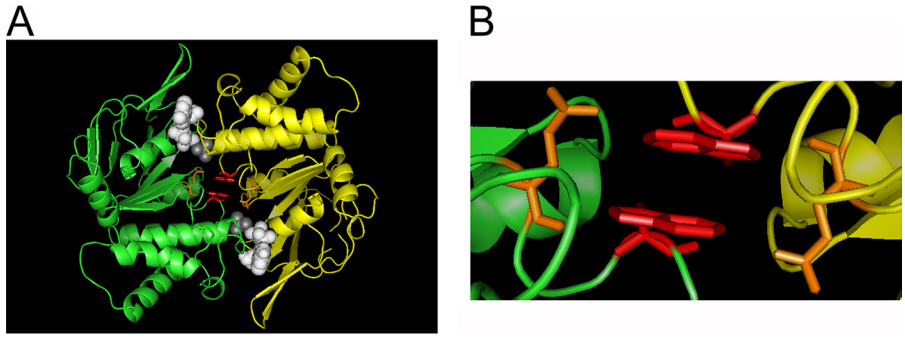

FIGURE 2. **Crystal structure of the MJI ADP sandwich dimer.** *A*, overall dimer structure. Ribbon representation of the two MJI monomers (in *green* and *yellow*), with the ADP (*white*) and P_i (*gray*) in a space-filling representation and a stick representation of Gln-171 (*orange*) and Trp-174 (*magenta*). *B*, view of the Trp-174 area showing the π-stacked Trps from the NBD monomers.

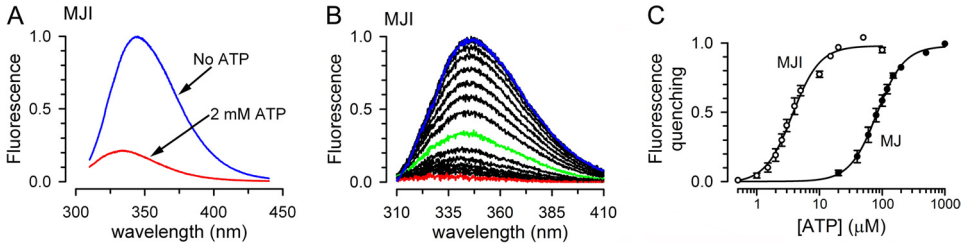

FIGURE 3. **ATP-dependent changes in Trp-174 fluorescence.** *A*, fluorescence spectra from MJI in the absence (*blue*) or presence of 2 mM ATP (*red*). The solutions were nominally divalent cation-free and contained 1 mM EDTA. Excitation wavelength was 295 nm. Buffer-only data were subtracted, and the data were normalized to the peak fluorescence in the absence of ATP. *B*, dependence of MJI Trp fluorescence on [ATP]. Fluorescence spectra were collected as in *A*, but varying [ATP] from zero (*blue*) to 1 mM (*red*). Intermediate [ATP] were 0.5, 1, 1.5, 2, 2.5, 3, 4, 5, 10 (*green*), 15, 20, 50, 100, 200, and 500 μM. There was a 5-min interval between the sequential ATP additions. Traces correspond to differences with the 2 mM-ATP data and were normalized to the peak emission in the absence of ATP. *C*, summary of the ATP dependence of MJ and MJI Trp quenching. The fractional maximum fluorescence decrease from experiments similar to that in *B* is presented as mean ± S.E. The calculated K_d and Hill coefficient were 83.9 ± 8.1 μM and 2.0 ± 0.2 for MJ (n = 4, 3 independent purifications) and 4.2 ± 0.6 μM and 1.7 ± 0.1 for MJI (n = 3, 3 independent purifications).

dependence of Trp fluorescence quenching on ATP. The K_d for ATP was ~20-fold higher for MJ than for MJI (84 μM *versus* 4 μM, respectively), and both proteins showed a similar cooperative response with Hill coefficients of 2.0 (MJ) and 1.7 (MJI). An increase in affinity for ATP by the Glu-171 to Gln substitution has been described previously (18).

Time Course of the ATP-dependent NBD Dimerization—The results above demonstrated that Trp174 quenching occurs as a consequence of ATP-induced dimerization and can therefore be used to follow this phenomenon. Fig. 4*A* shows the time course of the Trp fluorescence change in response to 2 mM ATP. Dimerization of MJ and MJI proceeded slowly, requiring > 3 min for completion. This long time to reach equilibrium is intrinsic to the system and not caused by poor mixing because the fluorescence quenching was still slow after rapid mixing in a stop-flow chamber (Fig. 4*B*). Trp-174 fluorescence quenching induced by 2 mM ATP was well fit by a two-exponential decay function with time constants (τ) τ_1 = 18.6 ± 1.6 and τ_2 = 103.2 ± 12.4 s for MJ (n = 3, fast component = 33 ± 6%) and τ_1 = 11.3 ± 1.9 and τ_2 = 63.1 ± 3.7 s for MJI (n = 3, fast component = 55 ± 5%). Because the rate of fluorescence quenching follows the decrease in concentration of monomeric NBDs as they dimerize, the data indicate that it takes minutes for all the NBDs to become dimers. This slow ATP-induced dimerization could be the result of a slow association rate or a fast dissociation rate. Our size-exclusion chromatography experiments showed that during the > 30 min that the preformed dimers were run in a column without ATP, all MJI and ~50% of MJ NBDs remained in the dimeric from (Fig. 1). These results suggest that dimer dissociation is very slow. Therefore, we can conclude that the slow dimerization is due to a slow association rate of the NBDs.

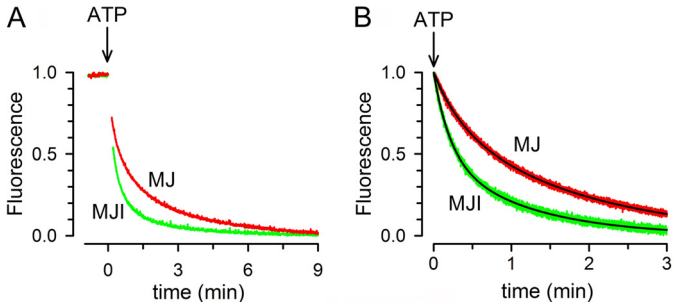

FIGURE 4. **Time course of dimerization.** *A*, effects of ATP on Trp-174 fluorescence quenching (*red*, MJ; *green*, MJI). The signals were normalized to the maximal change. The protein concentration was 2 μM. See "Experimental Procedures" for details. *B*, time course of Trp-174 fluorescence quenching by ATP after rapid mixing. MJ (*red*) or MJI (*green*) were mixed on a stop-flow apparatus with an equal volume of buffer containing ATP, and the decrease in Trp fluorescence was monitored. The final concentrations of protein and ATP were 2 μM and 2 mM, respectively. *Black lines* are exponential fits to the data (see text). The records in both panels are representative from at least three similar experiments. All solutions were nominally divalent cation-free and contained 1 mM EDTA.

Dimer Dissociation following ATP Hydrolysis—To determine the consequences of ATP hydrolysis on dimer dissociation, we studied the effect of Mg on the dissociation of preformed dimers. When MJ was first dimerized by addition of 2 mM ATP, addition of 10 mM $MgCl_2$ induced a rapid increase in Trp-174 fluorescence (Fig. 5*A*, *red trace*). The rate of increase in Trp fluorescence determined from rapid mixing of preformed

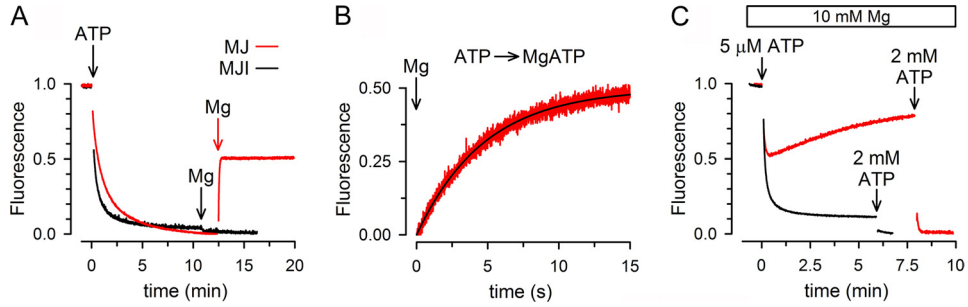

FIGURE 5. **Time course of the monomer/dimer equilibration following ATP hydrolysis.** *A*, effects of ATP and MgATP on MJ (*red*) and MJI (*black*) Trp-174 fluorescence. The first (*black*) and second (*red*) Mg-labeled *arrows* indicate the addition of $MgCl_2$ to MJI and MJ, respectively. The final concentrations of MJ or MJI, ATP, and Mg were 2 μM, 2 mM, and 10 mM, respectively. *B*, time course of the Trp-174 fluorescence increase elicited by MgATP after rapid mixing. MJ incubated with 2 mM ATP was mixed on a stop-flow apparatus with an equal volume of buffer containing MgATP, and the changes in Trp fluorescence were followed. The final concentrations of MJ, ATP, and Mg were 2 μM, 2 mM, and 10 mM, respectively. The *black line* is a single-exponential fit to the data. *C*, response of MJ Trp-174 fluorescence to low [MgATP]. MJ was exposed to 10 mM Mg and then 5 μM ATP followed by 2 mM ATP. The concentrations of MJ and MJI in all panels were 2 μM, and the records are representative of data from at least four similar experiments.

dimers (in 2 mM ATP) with Mg (Fig. 5*B*) can be fitted by a single exponential function with $\tau = 4.1 \pm 0.6$ s ($n = 4$). This value yields a rate constant of 0.24 s, which is close to the measured MJ0796 ATPase activity (~0.2 s) (25). Interestingly, addition of Mg did not return the fluorescence to the value before addition of ATP (where all NBD were monomers, Fig. 5*A*). Instead, MgATP induced a new steady state that consistently reached halfway between the monomer and dimer signals (Fig. 5*A*), suggesting that under this condition only 50% of the NBDs are monomers. The effect of Mg was absent in MJI (Fig. 5*A*, *black trace*), which suggests that the dissociation of the MJ dimers depended on ATP hydrolysis.

Additional evidence for the coupling of ATP hydrolysis and dimer dissociation is presented in Fig. 5*C*. In the presence of 10 mM Mg, a low concentration of ATP (5 μM) induces a rapid and transitory dimerization of MJ (Fig. 5*C*, *red trace*). After reaching a minimum, fluorescence slowly returned toward the value it had before addition of ATP. Because the affinity of MJ for MgATP is ~15-fold higher than its affinity for NaATP (~5 μM *versus* ~80 μM, respectively, see supplemental Figs. 2 and 3*C*), low concentrations of MgATP can induce the observed initial dimerization. There was no fluorescence recovery at saturating concentrations of ATP (see Fig. 5*C*, *red trace*, after addition of 2 mM ATP). Contrarily, addition of 5 μM ATP to MJI was enough to produce a stable dimerization, similar to the one produced by 2 mM ATP (Fig. 5*C*, *black trace*). These results suggest that ATP hydrolysis with the resulting release of hydrolysis products accelerates dimer dissociation and, as the concentration of MgATP decreases, less NBDs reassociate. This is expected because ADP cannot induce MJ dimerization (25). At 2 mM ATP, hydrolysis is insufficient to reduce the MgATP concentration below the saturation level. In summary, we interpret the results as an indication of reversible dimerization and dissociation of MJ in the presence of ATP hydrolysis. These results also suggest that we can follow in real time the association/dissociation cycle of a catalytically active NBD.

NBD Dimerization in the Presence of MgATP—The rapid monomer/dimer equilibrium that follows ATP hydrolysis (Fig. 5) is not compatible with the slow ATP-induced dimerization observed for MJ (Fig. 4) because the slow process should dominate the equilibration kinetics, and the steady-state concentration of monomers will be much higher than that of dimers. One possibility to explain the discrepancy between the slow ATP-induced dimerization and the fast monomer/dimer equilibration in the presence of MgATP is that the dimerization induced by MgATP occurs faster than that induced by NaATP. To test this possibility, we determined the speed of dimerization induced by MgATP. Fig. 6*A* illustrates that upon rapid mixing of MJ with 2 mM MgATP, Trp, fluorescence quenching was much more rapid (*red trace*) than upon mixing MJ with NaATP (*green trace*). Indeed, the new steady state was reached in ~10 s with MgATP as opposed to > 3 min with ATP without Mg (see also Fig. 4). The decrease in Trp fluorescence after addition of MgATP was well fit by a single-exponential decay function with a τ of 4.3 ± 1.3 s ($n = 4$), indicating that dimerization induced by MgATP occurred at a similar speed than the Mg-induced dimer dissociation ($\tau = 4.3$ s *versus* $\tau = 4.1$ s, not statistically different, see supplemental Table 2). Fig. 6*A* also shows that the total fluorescence quenching with MgATP (*red trace*, *right scale*) was about 50% of the quenching with NaATP (*green trace*, *left scale*). Because at 2 mM ATP essentially all NBD are dimers, the new steady state fluorescence value obtained with MgATP indicates ~50% monomers in the NBD population. As shown above (Fig. 5*A*), a similar 50% fluorescence level was reached after addition of Mg to preformed dimers. These results indicate that the new steady state reached in the presence of MgATP did not depend on the starting populated species. Starting with either 100% monomers or 100% dimers, a ~50% monomer population was reached with a τ of ~4 s. We therefore conclude that in the presence of saturating MgATP, NBDs associate and dissociate rapidly, reaching a dynamic equilibrium where approximately half of the molecules are dimers and half monomers.

The effect of Mg on MJI dimerization was also studied. Fig. 6*B* shows that the acceleration of MJI dimerization by MgATP *versus* NaATP alone was minimal and that in both cases complete quenching was reached, suggesting that all molecules became dimers. The decrease in MJI Trp fluorescence after addition of MgATP was well fit by a two-exponential decay function with $\tau_1 = 6.8 \pm 0.1$ and $\tau_2 = 43.3 \pm 0.9$ s ($n = 4$, fast component = 68 ± 1%) that was only ~50% faster than the dimerization in response to NaATP (see supplemental Table 2 for comparison). A similar slow dimerization induced by MgATP has been reported before for a catalytically inactive

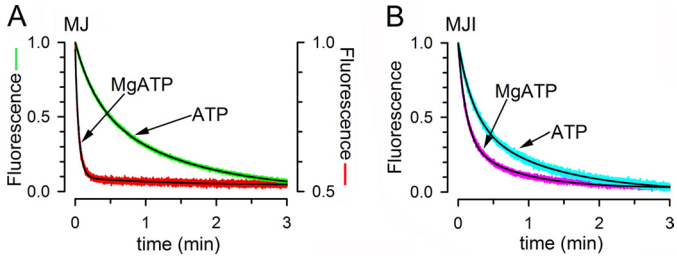

FIGURE 6. **Effect of Mg on the monomer/dimer equilibration.** *A*, time course of MJ Trp-174 fluorescence quenching by ATP (*green*) and MgATP (*red*) after rapid mixing. Unlabeled MJ was mixed on a stop-flow apparatus with an equal volume of buffer with ATP alone or MgATP, and the decrease in Trp fluorescence was followed. The final concentrations of MJ, ATP, and Mg were 2 μM, 2 mM, and 10 mM, respectively. Data were normalized to the total Trp quenching, which for MJ in MgATP was ~50% of the other values (see Fig. 5*A*). *B*, time course of MJI Trp-174 fluorescence quenching by ATP (*cyan*) and MgATP (*pink*) after rapid mixing. The experimental protocol was the same as that in *A*. The concentration of MJI was 2 μM. The *black lines* in *A* and *B* are exponential fits to the data (see text). The records in *A* and *B* are representative data from at least three similar experiments.

NBD equivalent to MJI (23). The limited acceleration of MJI dimerization by MgATP suggests that kinetic studies in E171Q and equivalent NBD mutants cannot be extrapolated to catalytically active proteins under hydrolysis conditions.

DISCUSSION

In this study, we developed a robust spectroscopic approach to assess dimerization of an ABC-protein NBD and employed it to study for the first time the steady state and kinetics of the monomer/dimer cycle in a catalytically active NBD.

The elucidation of the structural basis of the ATP-dependent Trp-174 fluorescence quenching presented here establishes Trp-174 as a NBD dimerization probe, opening the possibility of using a Trp at the equivalent position of other ABC proteins to monitor NBD dimerization. The residue at position 174 in MJ is not conserved among ABC proteins, but it is just two residues away from a conserved acidic residue at the end of the Walker B motif (Glu-171 in MJ0796).

In the absence of ATP, the Trp-174 emission maximum of 345 nm is consistent with solvent exposure, as expected from the equivalent Gly-174 position in the MJ0796 monomer structure (27). The blue shift in the emission maximum in high ATP concentration is consistent with the more hydrophobic environment of the dimer interface (28). In support of this conclusion, our MJI structure shows π stacking (**1p**, *parallel configuration*) of the Trp-174 residues of each monomer near the center of the dimer interface. Because the distance between the Trp rings is 3.0–3.5 Å, energy transfer is expected to make a significant contribution to the fluorescence quenching because this distance is shorter than the Förster distance for Trp-Trp FRET homotransfer (R_0 estimated at 4–16 Å) (29). However, other mechanisms such as static quenching (30) are also likely to play a role.

In aromatic interactions such as the Trp-Trp in the MJI dimer, van der Waals forces seem to dominate the binding interaction, with a minor, probably repulsive, electrostatic contribution (31). At a distance of 3.0–3.5 Å between the aromatic rings, the Trp-Trp binding energy could be as much as 3 kcal/mol (31). This could account for the increased dimer stability that allowed us to see for the first time MJ dimers in the size exclusion chromatography and kinetic experiments.

The MJI structure with ADP sandwiched at the dimer interface is very similar to that of ATP-bound MJ0796-E171Q (18). Because ADP does not promote dimerization of MJI (25) the two ADPs found in our structure must originate from ATP hydrolysis. The presence of a stable dimer with bound ADP and P_i strongly suggests that dimer dissociation requires release of the hydrolysis products. The high stability of the MJI dimer in the size exclusion chromatography experiments, and the observation of the hydrolysis products in the crystal structure, suggest that the slow release of ATP hydrolysis products contributes to the very low ATPase activity of MJI. Independently of the relevance of this finding for the catalytic mechanism, the new dimer structure with the hydrolysis products in the active site represents a structural intermediate state of the NBD ATPase cycle: post-hydrolysis and before ADP release.

Our kinetics studies on the Trp-174 proteins showed slow dimerization for MJI and also for MJ in the absence of Mg, comparable with a previous report of the time course of NBD dimerization of a catalytically deficient mutant equivalent to MJI (23). In that study, dimerization was detected by FRET self-quenching of a fluorescent probe bound to a C-terminal poly His tag. This slow association of ATP-bound monomers in the absence of ATP hydrolysis (E171Q mutation or absence of Mg in the case of the active NBDs) is due to the process of dimerization itself because it is not limited by the concentration of NBD, as demonstrated by the fast monomer/dimer equilibration elicited by MgATP in the catalytically active MJ. In addition to being slower, the dimerization observed in the absence of ATP hydrolysis shows more complex kinetics with two clearly defined rates. This could be explained by the presence of two nucleotide-free NBDs and/or NBD-ATP populations with a different ability to dimerize, which become more uniform in a MgATP-bound, "dimerization-ready" conformation. The different crystal conformations of NBDs in the absence of nucleotides and NMR data support the idea of an ensemble of pre-existing apo states (27, 32–34).

In this work, we were able to carry out kinetic experiments in a catalytically active ABC NBD for the first time, and the results show that the NBDs in mM MgATP rapidly reach a monomer/dimer dynamic equilibrium. We interpret the finding that MgATP yields a fluorescence value intermediate between that of 100% monomers and 100% dimers (see Figs. 5*A* and 6*A*) as the result of a dynamic equilibrium where approximately half of the NBDs are monomers and half form dimers. Alternatively, a similar fluorescence value could be the result of opening of the dimers in a way that increases the distance between the Trps, reducing quenching. Our size exclusion chromatography data in the presence of MgATP did not result in a well defined dimer peak but in a broad peak that can be interpreted as a dynamic mix of monomers and dimers with an intermediate apparent molecular mass (supplemental Fig. 1). Therefore, we conclude that the intermediate MJ Trp fluorescence in MgATP (*versus* NaATP or Apo ATP-free MJ) arises from a dynamic steady state with similar monomer and dimer concentrations as opposed to a population of partially opened dimers. In our experiments, after addition of saturating MgATP to MJ, the

monomer concentration (M) decreased from 2 to 1 μM, and the dimer concentration (D) increased from 0 to 0.5 μM (D = 2 M). Because the M and D populations at equilibrium are very close, neither dimerization nor dimer dissociation are clearly favored. This analysis is valid only for MJ with mM MgATP, where the hydrolysis-dependent increase in dimer dissociation is accompanied by fast redimerization. MJ dimerization occurs slowly if NaATP is used instead of MgATP. In the case of MJI, Mg has a reduced accelerating effect on dimerization, which is in agreement with a report of reduced MgATP *versus* NaATP selectivity of the MJ0796-E171Q mutant (18). Although the molecular events responsible for the faster MgATP- *versus* NaATP-induced dimerization of MJ are not definitively established, Mg coordination at the active site and electrostatics at the dimer interface are likely to play a role (18). In a number of NTPases, including ABC NBDs, the conserved acidic residue at the end of the Walker B motif (Glu-171 in MJ0796) makes a water-mediated contact to Mg. This is required for high-affinity nucleotide binding to a number of NTPases (35, 36). A similar structural arrangement can contribute to the increased affinity of MJ for MgATP *versus* NaATP. In addition, the nucleotide-bound dimer interface has a relatively intense concentration of negative charge, and Mg could facilitate NBD association by reducing the negative charge of the ATP. This can also explain why the dimerization induced by MgATP is faster than that induced by NaATP.

Our findings suggest that previous estimates of NBD association rates, obtained in catalytically deficient mutants (equivalent to MJI), underestimate the true rates in catalytically active NBDs in mM MgATP ("physiological conditions"). In the poorly active NBDs, the rate of ATP-induced dimer formation dominates the kinetics of the monomer/dimer cycle, and the equilibrium concentration of monomers is close to zero. In catalytically active NBDs, dimer formation and dissociation are faster, and the equilibrium concentrations of monomer and dimer are very similar. Given the high effective NBD concentration in full-length ABC proteins, which will potentially increase the speed of NBD association, ATP hydrolysis could be the rate-limiting step of the cycle in most cases. However, this argument assumes no structural constraints from transmembrane domains/intracellular loops and does not consider that hydrolysis rates of ABC proteins are highly variable. They range from relatively low rates of 0.2 s (*e.g.* CFTR) (37) to ~50-fold faster rates (*e.g.* P-glycoprotein at 10 s) (38). Therefore, the rate-limiting step of the hydrolysis cycle may differ among ABC proteins.

Acknowledgments—We thank Drs. Luis Reuss and Ina Urbatsch, as well as Rebecca Cooper-Sisson, Ellen Hildebrandt, and Srinivasan Krishnan for discussions and comments on the manuscript. We also thank Catherine Hamilton for technical assistance. Portions of this research were carried out at the Stanford Synchrotron Radiation Lightsource, a Directorate of SLAC National Accelerator Laboratory and an Office of Science User Facility operated for the United States Department of Energy Office of Science by Stanford University.

REFERENCES

1. Bouige, P., Laurent, D., Piloyan, L., and Dassa, E. (2002) Phylogenetic and functional classification of ATP-binding cassette (ABC) systems. *Curr. Protein Pept. Sci.* **3,** 541–559
2. Sharom, F. J. (2008) ABC multidrug transporters. Structure, function and role in chemoresistance. *Pharmacogenomics* **9,** 105–127
3. Davidson, A. L., Dassa, E., Orelle, C., and Chen, J. (2008) Structure, function, and evolution of bacterial ATP-binding cassette systems. *Microbiol. Mol. Biol. Rev.* **72,** 317–364
4. Senior, A. E., al-Shawi, M. K., Urbatsch, I. L. (1995) The catalytic cycle of P-glycoprotein. *FEBS Lett.* **377,** 285–289
5. Csanády, L. (2010) Degenerate ABC composite site is stably glued together by trapped ATP. *J. Gen. Physiol.* **135,** 395–398
6. Borbat, P. P., Surendhran, K., Bortolus, M., Zou, P., Freed, J. H., and Mchaourab, H. S. (2007) *PLoS Biol.* **5,** 2211–2219
7. Chen, J., Lu, G., Lin, J., Davidson, A. L., and Quiocho, F. A. (2003) A tweezers-like motion of the ATP-binding cassette dimer in an ABC transport cycle. *Mol. Cell* **12,** 651–661
8. Dawson, R. J., and Locher, K. P. (2006) Structure of a bacterial multidrug ABC transporter. *Nature* **443,** 180–185
9. Higgins, C. F. (2007) Multiple molecular mechanisms for multidrug resistance transporters. *Nature* **446,** 749–757
10. Hopfner, K. P., Karcher, A., Shin, D. S., Craig, L., Arthur, L. M., Carney, J. P., and Tainer, J. A. (2000) Structural biology of Rad50 ATPase. ATP-driven conformational control in DNA double-strand break repair and the ABC-ATPase superfamily. *Cell* **101,** 789–800
11. Hwang, T. C., and Sheppard, D. N. (2009) Gating of the CFTR Cl- channel by ATP-driven nucleotide-binding domain dimerisation. *J. Physiol.* **587,** 2151–2161
12. Janas, E., Hofacker, M., Chen, M., Gompf, S., van der Does, C., and Tampé, R. (2003) The ATP hydrolysis cycle of the nucleotide-binding domain of the mitochondrial ATP-binding cassette transporter Mdl1p. *J. Biol. Chem.* **278,** 26862–26869
13. Jones, P. M., and George, A. M. (2007) Nucleotide-dependent allostery within the ABC transporter ATP-binding cassette. A computational study of the MJ0796 dimer. *J. Biol. Chem.* **282,** 22793–227803
14. Jones, P. M., and George, A. M. (2009) Opening of the ADP-bound active site in the ABC transporter ATPase dimer: evidence for a constant contact, alternating sites model for the catalytic cycle. *Proteins* **75,** 387–396
15. Jones, P. M., and George, A. M. (2011) Molecular-dynamics simulations of the ATP/apo state of a multidrug ATP-binding cassette transporter provide a structural and mechanistic basis for the asymmetric occluded state. *Biophys. J.* **100,** 3025–3034
16. Oswald, C., Holland, I. B., and Schmitt, L. (2006) The motor domains of ABC-transporters. What can structures tell us? *Naunyn-Schmiedeberg's Arch. Pharmacol.* **372,** 385–399
17. Sauna, Z. E., Kim, I. W., Nandigama, K., Kopp, S., Chiba, P., and Ambudkar, S. V. (2007) Catalytic cycle of ATP hydrolysis by P-glycoprotein. Evidence for formation of the E.S. reaction intermediate with ATP-γ-S, a nonhydrolyzable analogue of ATP. *Biochemistry* **46,** 13787–13799
18. Smith, P. C., Karpowich, N., Millen, L., Moody, J. E., Rosen, J., Thomas, P. J., and Hunt, J. F. (2002) ATP binding to the motor domain from an ABC transporter drives formation of a nucleotide sandwich dimer. *Mol. Cell* **10,** 139–149
19. Ward, A., Reyes, C. L., Yu, J., Roth, C. B., and Chang, G. (2007) Flexibility in the ABC transporter MsbA. Alternating access with a twist. *Proc. Natl. Acad. Sci. U.S.A.* **104,** 19005–19010
20. Westfahl, K. M., Merten, J. A., Buchaklian, A. H., and Klug, C. S. (2008) Functionally important ATP binding and hydrolysis sites in *Escherichia coli* MsbA. *Biochemistry* **47,** 13878–13886
21. Vergani, P., Lockless, S. W., Nairn, A. C., and Gadsby, D. C. (2005) CFTR channel opening by ATP-driven tight dimerization of its nucleotide-binding domains. *Nature* **433,** 876–880
22. Sauna, Z. E., and Ambudkar, S. V. (2007) About a switch. How P-glycoprotein (ABCB1) harnesses the energy of ATP binding and hydrolysis to do mechanical work. *Mol. Cancer Ther.* **6,** 13–23
23. van der Does, C., Presenti, C., Schulze, K., Dinkelaker, S., and Tampé, R.

(2006) Kinetics of the ATP hydrolysis cycle of the nucleotide-binding domain of Mdl1 studied by a novel site-specific labeling technique. *J. Biol. Chem.* **281,** 5694–56701
24. Zaitseva, J., Jenewein, S., Jumpertz, T., Holland, I. B., and Schmitt, L. (2005) H662 is the linchpin of ATP hydrolysis in the nucleotide-binding domain of the ABC transporter HlyB. *EMBO J.* **24,** 1901–1910
25. Moody, J. E., Millen, L., Binns, D., Hunt, J. F., and Thomas, P. J. (2002) Cooperative, ATP-dependent association of the nucleotide binding cassettes during the catalytic cycle of ATP-binding cassette transporters. *J. Biol. Chem.* **277,** 21111–21114
26. Narita, S., and Tokuda, H. (2006) An ABC transporter mediating the membrane detachment of bacterial lipoproteins depending on their sorting signals. *FEBS Lett.* **580,** 1164–1170
27. Karpowich, N., Martsinkevich, O., Millen, L., Yuan, Y. R., Dai, P. L., MacVey, K., Thomas, P. J., and Hunt, J. F. (2001) Crystal structures of the MJ1267 ATP binding cassette reveal an induced-fit effect at the ATPase active site of an ABC transporter. *Structure* **9,** 571–586
28. Vivian, J. T., Callis, P. R. (2001) Mechanisms of tryptophan fluorescence shifts in proteins. *Biophys. J.* **80,** 2093–20109
29. Kayser, V., Chennamsetty, N., Voynov, V., Helk, B., and Trout, B. L. (2011) Tryptophan-tryptophan energy transfer and classification of tryptophan residues in proteins using a therapeutic monoclonal antibody as a model. *J. Fluoresc.* **21,** 275–288
30. Chen, R. F., Knutson, J. R., Ziffer, H., and Porter, D. (1991) Fluorescence of tryptophan dipeptides. Correlations with the rotamer model. *Biochemistry* **30,** 5184–5195
31. McGaughey, G. B., Gagné, M., Rappé, A. K. (1998) π-Stacking interactions. Alive and well in proteins. *J. Biol. Chem.* **273,** 15458–15463
32. Schmitt, L., Benabdelhak, H., Blight, M. A., Holland, I. B., and Stubbs, M. T. (2003) Crystal structure of the nucleotide-binding domain of the ABC-transporter haemolysin B. Identification of a variable region within ABC helical domains. *J. Mol. Biol.* **330,** 333–342
33. Verdon, G., Albers, S. V., Dijkstra, B. W., Driessen, A. J., and Thunnissen, A. M. (2003) Crystal structures of the ATPase subunit of the glucose ABC transporter from *Sulfolobus solfataricus*. Nucleotide-free and nucleotide-bound conformations. *J. Mol. Biol.* **330,** 343–358
34. Wang, C., Karpowich, N., Hunt, J. F., Rance, M., and Palmer, A. G. (2004) Dynamics of ATP-binding cassette contribute to allosteric control, nucleotide binding and energy transduction in ABC transporters. *J. Mol. Biol.* **342,** 525–537
35. Leipe, D. D., Wolf, Y. I., Koonin, E. V., and Aravind, L. (2002) Classification and evolution of P-loop GTPases and related ATPases. *J. Mol. Biol.* **317,** 41–72
36. Sprang, S. R. (1997) G protein mechanisms. Insights from structural analysis. *Annu. Rev. Biochem.* **66,** 639–678
37. Ramjeesingh, M., Ugwu, F., Stratford, F. L., Huan, L. J., Li, C., and Bear, C. E. (2008) The intact CFTR protein mediates ATPase rather than adenylate kinase activity. *Biochem. J.* **412,** 315–321
38. Urbatsch, I. L., al-Shawi, M. K., and Senior, A. E. (1994) Characterization of the ATPase activity of purified Chinese hamster P-glycoprotein. *Biochemistry* **33,** 7069–7076
39. Moody, J. E. (2006) Characterization of the reaction cycle of MJ0796: A model archaeal adenosine triphosphate-binding cassette transporter nucleotide binding domain. Ph.D. thesis, University of Texas Southwestern Medical Center at Dallas, Dallas, TX

SUPPLEMENTARY INFORMATION

Kinetics of the association/dissociation cycle of an ATP-binding cassette nucleotide-binding domain

Maria E. Zoghbi, Kerry L. Fuson, Roger B. Sutton, and Guillermo A. Altenberg

Department of Cell Physiology and Molecular Biophysics, and Center for Membrane Protein Research, Texas Tech Health Sciences Center, Lubbock, TX 79430-6551, USA.

SUPPLEMENTARY FIGURES

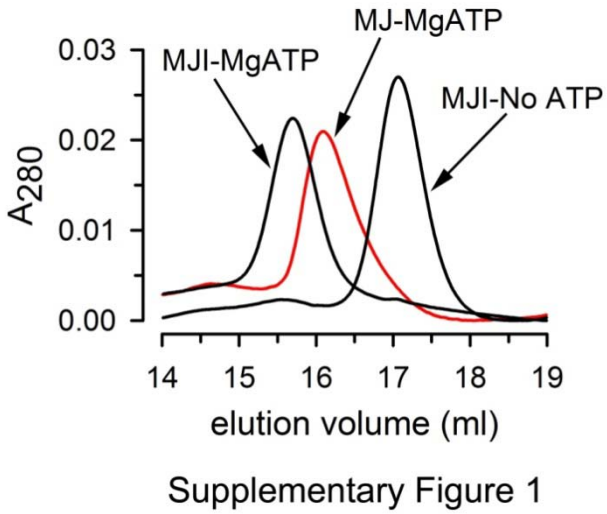

Supplementary Fig. 1. Size exclusion chromatography of purified MJ and MJI. MJ (red trace, labeled MJ-MgATP) preincubated with 1 mM ATP and 10 mM $MgCl_2$ was run on a column with 1 mM ATP and 10 mM $MgCl_2$. MJI preincubated and run in the absence of ATP (black trace, labeled MJI-No ATP) or in the presence of MgATP (black trace, labeled MJI-MgATP) is shown for comparison. See main text Fig. 1 and **Experimental Procedures** for details.

Supplementary Fig. 2. Dependence of MJ Trp174 fluorescence on MgATP. The fractional decrease in fluorescence is shown as means ± SEM. The calculated Kd was 5.4 ± 1.6 μM and the Hill coefficient was 1.0 ± 0.1 (n = 4). The effect of ATP alone on MJ Trp fluorescence is also shown for comparison (main text Fig. 3C). Fluorescence at varying concentrations of ATP was measured in 10 mM Mg. ATP was added at 30-s intervals, before reversal of the fluorescence quenching was evident (see main text Fig. 5C). MJ concentration was 0.5 or 2 μM.

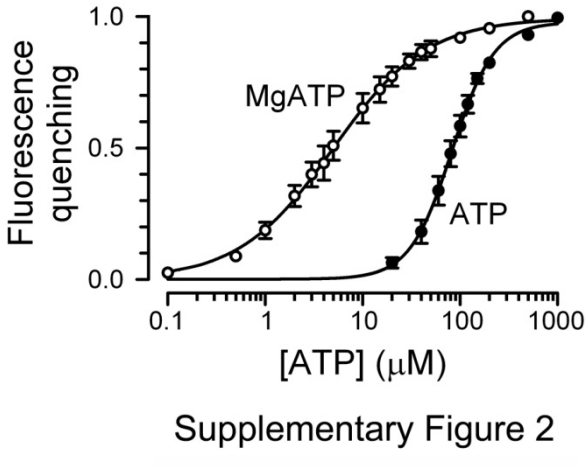

Supplementary Table 1
Data collection and refinement statistics

Parameters	Values
Data Collection Statistics[a]	
Space Group	$C222_1$
Unit Cell Parameters	80.6 Å, 106.3 Å, 117.2 Å 90°, 90°, 90°
Temperature (K)	100
Wavelength (Å)	0.9796
Resolution (Å)	33.3 – 1.8
R_{merge} (%)	5.5 (76)
Completeness (%)	99.6 (95.1)
$I / \sigma(I)$	36 (2.8)
Unique Reflections	46824
Redundancy	6.2
No. of molecules in the ASU	1
Refinement Statistics	
Resolution (Å)	33.3 – 1.8
Working Set	
No. of reflections	43167
R-factor (%)	18.73
Test Set	
No of reflections	3651
R-factor (%)	21.5
Protein atoms	3692
Non-protein atoms	82
Water molecules	206
Geometry Statistics	
r.m.s deviations in bonds (Å)	0.004
r.m.s. deviations in angles (°)	0.989
Ramachandran Plot	
Most favored Region (%)	98.7
Additionally allowed region (%)	1.3
Disallowed Region (%)	0
Protein Data Bank Code	3TIF

Supplementary Table 2
Summary of fits obtained from the stop-flow data, as presented in the main text

Conditions	MJ				MJI			
	A1 (%)	τ_1 (s)	τ_2 (s)	n	A1 (%)	τ_1 (s)	τ_2 (s)	n
No ATP to ATP	33 ± 6	18.6 ± 1.6	103.2 ± 12.4	3	55 ± 5	11.3 ± 1.9	63.1 ± 3.7	3
No ATP to MgATP	100	4.3 ± 1.3		4	68 ± 1	6.8 ± 0.1	43.3 ± 0.9	4
ATP to MgATP	100	4.1 ± 0.6		4		ND		4

A1 (%): faster or only exponential component calculated as: (A1/A1+A2) x 100; τ_1 and τ_2: lifetimes; No ATP: 1 mM EDTA/Mg-free; ATP: 2 mM ATP; MgATP: 2 mM MgATP; ND: not determined because there was no fluorescence change. Data are presented as means ± SEM, and n is the number of independent experiments.

Kinetics of the Association/Dissociation Cycle of an ATP-binding Cassette Nucleotide-binding Domain

Maria E. Zoghbi, Kerry L. Fuson, Roger B. Sutton and Guillermo A. Altenberg

J. Biol. Chem. 2012, 287:4157-4164.
doi: 10.1074/jbc.M111.318378 originally published online December 9, 2011
